Spherical transceivers for ultrafast optical wireless communications

Xian Jin, Blago A. Hristovski, Christopher M. Collier,
Simon Geoffroy-Gagnon, Brandon Born and Jonathan F. Holzman*
Integrated Optics Laboratory, School of Engineering, The University of British Columbia,
Kelowna, BC, Canada, V1V 1V7

ABSTRACT

Optical wireless communications (OWC) offers the potential for high-speed and mobile operation in indoor networks. Such OWC systems often employ a fixed transmitter grid and mobile transceivers, with the mobile transceivers carrying out bi-directional communication via active downlinks (ideally with high-speed signal detection) and passive uplinks (ideally with broad angular retroreflection and high-speed modulation). It can be challenging to integrate all of these bi-directional communication capabilities within the mobile transceivers, however, as there is a simultaneous desire for compact packaging. With this in mind, the work presented here introduces a new form of transceiver for bi-directional OWC systems. The transceiver incorporates radial photoconductive switches (for high-speed signal detection) and a spherical retro-modulator (for broad angular retroreflection and high-speed all-optical modulation). All-optical retro-modulation are investigated by way of theoretical models and experimental testing, for spherical retro-modulators comprised of three glasses, N-BK7, N-LASF9, and S-LAH79, having differing levels of refraction and nonlinearity. It is found that the spherical retro-modulator comprised of S-LAH79, with a refractive index of $n \approx 2$ and a Kerr nonlinear index of $n_2 \approx (1.8 \pm 0.1) \times 10^{-15}$ cm^2/W, yields both broad angular retroreflection (over a solid angle of 2π steradians) and ultrafast modulation (over a duration of 120 fs). Such transceivers can become important elements for all-optical implementations in future bi-directional OWC systems.

Keywords: All-optical networks, modulators, optical switching devices, optical wireless, ultrafast nonlinear optics.

1. INTRODUCTION

Optical wireless communications (OWC) is attractive for indoor networks[1,2], as it merges the high-speed transmission capability of optical communications with the mobility capability of wireless operations. Early generations of the OWC systems are emerging as Li-Fi[3] and free-space optical communications[4]. Unlike the contemporary fibre-optic networks, however, these OWC systems demand bi-directional operation between a central transceiver and widely-distributed transceivers[5]. Typically, the bi-directional OWC network employs an active downlink (having fixed LED[6] or laser[7] transceivers) broadcasting information to the remote transceivers, and a passive uplink (having the remote transceivers simultaneously modulating and redirecting the incident optical beams back to the fixed transceivers). The bi-directionality of retro-modulation in the passive links has numerous advantages, such as low power consumption, ease of deployment, and alignment insensitive[8,9]. However, there remains a challenge to implement effective retro-modulation, in terms of broad angular retroreflection and high-speed modulation, within a compact remote transceiver.

The broad angular retroreflection capability for effective retro-modulation can be implemented with the appropriate retroreflective structures, which can effectively redirect the incident optical beam back to its source in an antiparallel direction of its incidence. A singular corner-cube retroreflector (RR), with three mutually-orthogonal reflective surfaces, is often employed to do this, over a solid angle of $\pi/2$ steradians[10,11]. However, there is a demand for broader angular retroreflection[12] for OWC passive uplink operations. With this in mind, a spherical RR can be used[13,14], as it retroreflects over a full solid angle of 4π steradians. This is eight times broader than that of corner-cube RRs. However, the retroreflection process of a spherical RR is based on refraction, so it is necessary to have the spherical RR have an appropriate refractive index.

The high-speed modulation capability for effective retro-modulation can be implemented via the integration of external modulators. Mechanical modulators, using beam deflection[15], and electrical modulators, using liquid crystal absorption[4,16],

*jonathan.holzman@ubc.ca; phone 1-250-807-8798; fax 1-250-807-9850; iol.ok.ubc.ca

Optical Components and Materials XIII, edited by Shibin Jiang, Michel J. F. Digonnet,
Proc. of SPIE Vol. 9744, 97440F · © 2016 SPIE · CCC code: 0277-786X/16/$18
doi: 10.1117/12.2208343

have often been employed for the modulation but their millisecond-timescale modulation is not suited for high-speed OWC passive uplinks. Thus, an electrical modulator, using multiple-quantum-well absorption[8], was demonstrated. It provided nanosecond-timescale modulation to enable gigabit-per-second communication rates for high-speed OWC passive uplinks. To further improve the modulation rates, all-optical switches can be used, by having one (local) optical beam modulate the second (incident) optical beam by way of nonlinear optical interaction[17]. Such a process has the potential for high-speed modulation[18] on picosecond and femtosecond timescales. However, the operation is based on optical nonlinearity, so it is necessary to have the material exhibit a sufficiently high nonlinearity.

In this work, an integrated device is introduced to facilitate effective retro-modulation with broad angular retroreflection and high-speed modulation, for use in bi-directional OWC networks. The structure takes the form of a spherical RR (to enable broad angular retroreflection) and all-optical modulation (to enable high-speed modulation). Theoretical and experimental analyses are presented for three distinct spherical RRs, with differing refraction and nonlinearity, to characterize their retroreflection capabilities. The three spherical RRs are investigated via a time-resolved pump-probe setup to characterize their high-speed retro-modulation capabilities. It is found that the OWC transceiver with a S-LAH79 spherical RR is best-suited for OWC passive uplink operation, as it exhibits broad angular retroreflection and ultrafast retro-modulation.

2. DEVICE AND SYSTEM DESIGN

The desired retro-modulation can be met through the spherical transceiver shown in Fig. 1. The spherical transceiver consists of three voltage-biased photoconductive (PC) switches, mounted radially and equal-spaced on a thin aperture, and a spherical RR, mounted at the geometrical centre of the same thin aperture. A uniform and collimated 1550 nm signal beam is incident towards the spherical transceiver along the optical axis (OA) that is oriented with an azimuthal angle, ϕ, and polar angle, θ, according to the *xyz*-coordinate system shown in Fig. 1(a). The 1550 nm signal beam is incident across the three PC switches. The incident signal beam is sampled and summed by an electrical via-hole (not shown) for OWC active downlink reception[4,19]. The 1550 nm signal beam also gets refracted by the entrance interface of the spherical RR, then focused and reflected at the rear interface of the spherical RR, and ultimately re-collimated by the entrance interface of the spherical RR for its return back to its source. Meanwhile, the spherical transceiver uses its local 780 nm control beam (on the rear interface of the sphere) to modulate the incident 1550 nm signal beam. Isolation of the local 780 nm control beam is achieved by way of a 1550 nm dichroic filter (not shown) that passes the 1550 nm signal beam and blocks the local 780 nm control beam. The retroreflection process by the spherical RR and the nonlinear optical beam interaction at the rear surface of the spherical RR, together, support the desired retro-modulation.

To achieve the desired level of broad angular retroreflection and high-speed modulation characteristics, it is necessary to select the optical materials with appropriate refractive index, n, and nonlinear coefficient, n_2, respectively, for the spherical RR. Three representative optical materials are selected in this work for spherical RRs: N-BK7 with a small refractive index of $n = 1.51$ and a low nonlinear coefficient of $n_2 = 3.2 \times 10^{-16}$ cm^2/W; N-LASF9 with a moderate refractive index of $n = 1.85$ and a moderate nonlinear coefficient of $n_2 = 1.7 \times 10^{-15}$ cm^2/W; and S-LAH79 with a large refractive index of $n = 2.00$ and a high nonlinear coefficient of $n_2 = 2.8 \times 10^{-15}$ cm^2/W. The refractive indices, n, are defined by Schott glass data, and the nonlinear coefficients, n_2, are from calculations according to the Boling-Glass-Owyoung (BGO) model[20]. All three spherical RRs have a radius of $a = 2.5$ mm. All three glasses have a broad and constant transparency across the visible to near-infrared wavelengths, as shown in Fig. 2. This broad wavelength window covers the operational wavelengths of typical indoor visible light communication systems[21] as well as outdoor free-space optical communication systems[9].

3. THEORETICAL ANALYSES

Theoretical analyses are carried out in this section of the three selected glasses for the spherical RRs to characterize their refraction. This allows the material with the optimal refractive index (for retroreflection) to be selected. (An analogous characterization of nonlinearity of the spherical RRs is deemed to be unnecessary, as it is simply understood that a larger nonlinear coefficient improves the uplink performance[22].)

A ray-tracing model is used for the refractive index characterization. In this model, the spherical RR is illuminated by a collimated optical beam, with a uniform intensity, from a distant source along the OA. The optical beam is refracted at

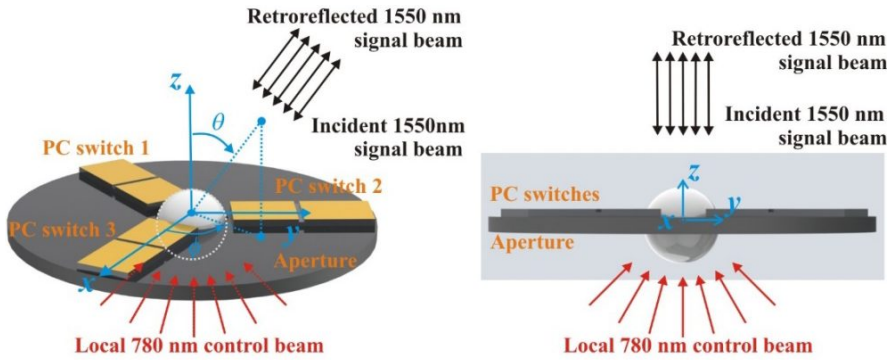

(a) (b)

Figure 1. Solidworks schematics of the spherical transceiver are shown as (a) an oblique view and (b) a cross-sectional view. The spherical transceiver consists of three radial photoconductive (PC) switches (performing ultrafast photodetection), a spherical retro-modulator (performing ultrafast retro-modulation), and a mounting aperture (blocking stray light). The collimated signal beams at a wavelength of 1550 nm illuminate the spherical transceiver along azimuthal, ϕ, and polar, θ, angles defined within the *xyz*-coordinate system. The signal beam is retroreflected back to its source. A local control beam at a wavelength of 780 nm illuminates the rear interface of the sphere to apply all-optical modulation to the signal beam.

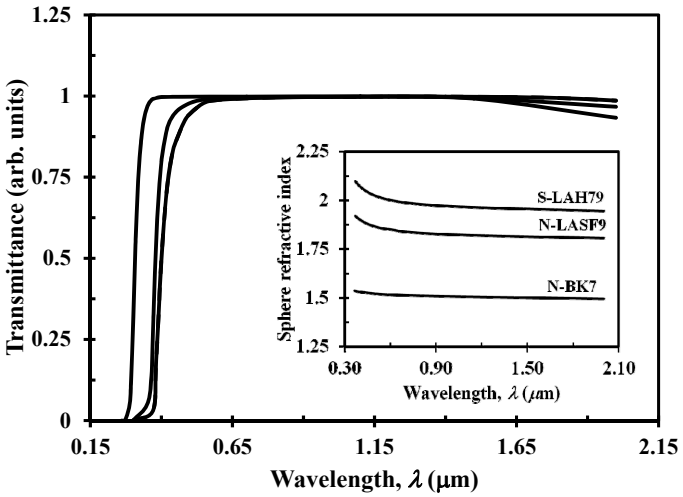

Figure 2. Transmittance is shown as a function of wavelength, λ, for N-BK7 (n = 1.51), N-LASF9 (n = 1.85), and S-LAH79 (n = 2.00) materials (from left to right). The figure inset shows the respective refractive index as a function of wavelength, λ, for N-BK7 (n = 1.51)[23], N-LASF9 (n = 1.85)[24], and S-LAH79 (n = 2.00)[25] materials.

the entrance interface and then focused at the rear interface of the spherical RR. The incident signal intensity, $I_{si}(z = -a)$, at the intersection of the OA and the rear interface of the spherical RR is investigated, and the normalized results are shown as a function of differing refractive index, n, in Fig. 3(a). It is clear that the S-LAH79 (n = 2.00) spherical RR can best focus the incoming optical beam at its rear interface, compared with the N-BK7 (n = 1.51) and N-LASF9 (n = 1.85) spherical RRs. This is beneficial for retroreflection as it will enable re-collimation as well as modulation (via an intense signal-control beam interaction). The normalized theoretical incident signal intensity results are seen to agree with the theoretical refraction approximation results of the spherical RRs[26], which suggests that the sphere with its refractive index of 2 best focus the paraxial light rays at the intersection of the OA and its rear interface. A similar conclusion can also be seen in our rigorous electromagnetic simulations[18] via Mie theory[27].

After being focused and reflected at the rear interface of the spherical RR, the optical beams are re-collimated by the entrance interface for return back to their sources along the OA. The retroreflection simulations and measurements are carried out over a propagation distance of $z = L$ = 3.00 m, and the normalized theoretical retroreflected signal intensity, $I_{sr}(z = L)$, are shown as a function of the refractive index, n, in Fig. 3(b). It is clear that the S-LAH79 (n = 2.00) spherical RR can best retroreflect the incoming optical beams, as its theoretical retroreflected signal intensity is approximately 1 ×

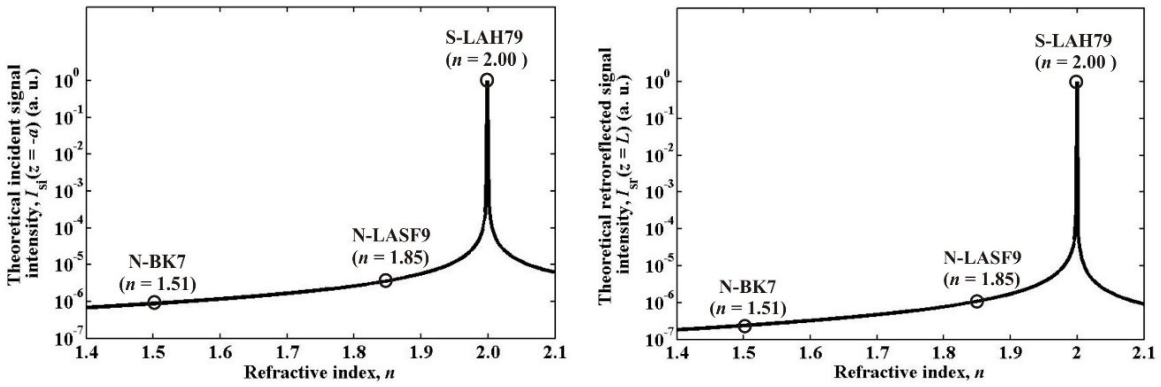

Figure 3. Theoretical normalized incident signal intensity, $I_{si}(z = -a)$, at the rear interface of the spherical RRs, and the retroreflected signal intensity, $I_{sr}(z = L)$, at the source are shown as a function of material refractive index, n, in (a) and (b), respectively, for N-BK7 (n = 1.51), N-LASF9 (n = 1.85), and S-LAH79 (n = 2.00) spherical RRs.

10^6 times larger than that of the N-LASF9 (n = 1.85) spherical RR and approximately 5×10^6 times larger than that of the N-BK7 (n = 1.51) spherical RR. These theoretical results are in good agreement with the experimental retroreflection measurements with spherical RRs[28]. Further tests of the S-LAH79 (n = 2.00) spherical RR show that its retroreflection region, being the central 3% of the sphere's cross-sectional area, exhibits a relatively small divergence angle of 0.02°.

4. EXPERIMENTAL RESULTS AND DISCUSSION

In the previous section, retroreflection was characterized for three spherical RRs, and it has shown that the S-LAH79 (n = 2.00) spherical RR can achieve the best refraction and retroreflection. To experimentally characterize the full all-optical retro-modulation, a time-resolved impulsive excitation setup is built and shown in Fig. 4. The local 780 nm control beam (red), with a pulse duration of 110 fs, illuminates the rear interface of the spherical transceiver with an intensity varying from 0.52 GW/cm^2 to 2.1 GW/cm^2. At the same time, the remote 1550 nm signal beam (yellow), with a pulse duration of 110 fs, illuminates the entrance interface of the spherical transceiver and is focused on its rear interface. For the time-resolved tests, the local 780 nm control pulses are delayed, by a motorized stage, with respect to the remote 1550 nm signal pulses. All-optical modulation occurs when the local 780 nm control beam and remote 1550 nm signal beam arrive at the rear interface of the spherical transceiver at the same time, t. The modulated 1550 nm signal beam is retroreflected by the spherical transceiver, sampled by a beamsplitter, and recorded by a distant photodetector.

The impulsive excitation results are shown as the retroreflected 1550 nm signal intensity, $I_s(t)$, as a function of the delay time, t, in Fig. 5. Figure 5(a) shows the retroreflected 1550 nm signal intensity, $I_s(t)$, for the N-BK7 (n = 1.51) spherical transceiver, Figure 5(b) shows the retroreflected 1550 nm signal intensity, $I_s(t)$, for the N-LASF9 (n = 1.85) spherical transceiver, and Figure 5(c) shows the retroreflected 1550 nm signal intensity, $I_s(t)$, for the S-LAH79 (n = 2.00) spherical transceiver. The retroreflected 1550 nm signal intensities are all normalized with respect to the signal intensity of the S-LAH79 (n = 2.00) spherical transceiver. It is clear that the S-LAH79 (n = 2.00) spherical transceiver achieves the highest level of retro-modulation, with its peak retro-modulated signal intensity about 1.33 times larger than that of the N-LASF9 (n = 1.85) spherical transceiver and approximately 5 times larger than that of the N-BK7 (n = 1.51) spherical transceiver. The time-domain retro-modulated signals in Fig. 5 also give insight into the all-optical modulation mechanism. All three retro-modulated signals are symmetric with respect to the zero-time with a full-width-at-half-maximum of approximately 120 fs, which is comparable with the pulse durations of both the local 780 nm control beam and the remote 1550 nm signal beams. Thus, it can be concluded that the nonlinear optical beam interaction at the rear interface of the spherical transceiver introduces a nonresonant nonlinearity, which is due to the nonlinear electronic polarization of the glasses (rather than resonant charge-carrier photogeneration and recombination[19]). When the local 780 nm control beam interacts with the remote 1550 nm signal beam on the rear interface of the spherical transceiver, a transient refractive index increase is established, and the retroreflected signal intensity increases due to the effect of the positive nonlinear coefficient, n_2. There also exist two small negative sidelobes, before and after the central peaks, in each figure of Fig. 5. This can be explained by the fact that the local 780 nm control beam interacts with the remote 1550 nm signal beam in the bulk of the sphere after and before the 1550 nm signal beam strikes the rear interface, respectively.

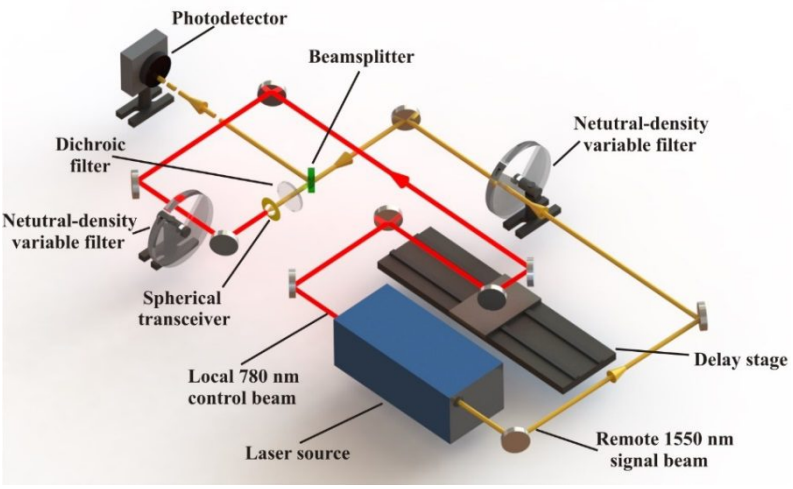

Figure 4. A schematic of the time-resolved impulsive excitation setup is shown (not to scale). The retroreflected 1550 nm signal intensity, $I_s(t)$, is recorded at the photodetector as a function of the time delay, t, between the local 780 nm control beam and remote 1550 nm signal beam.

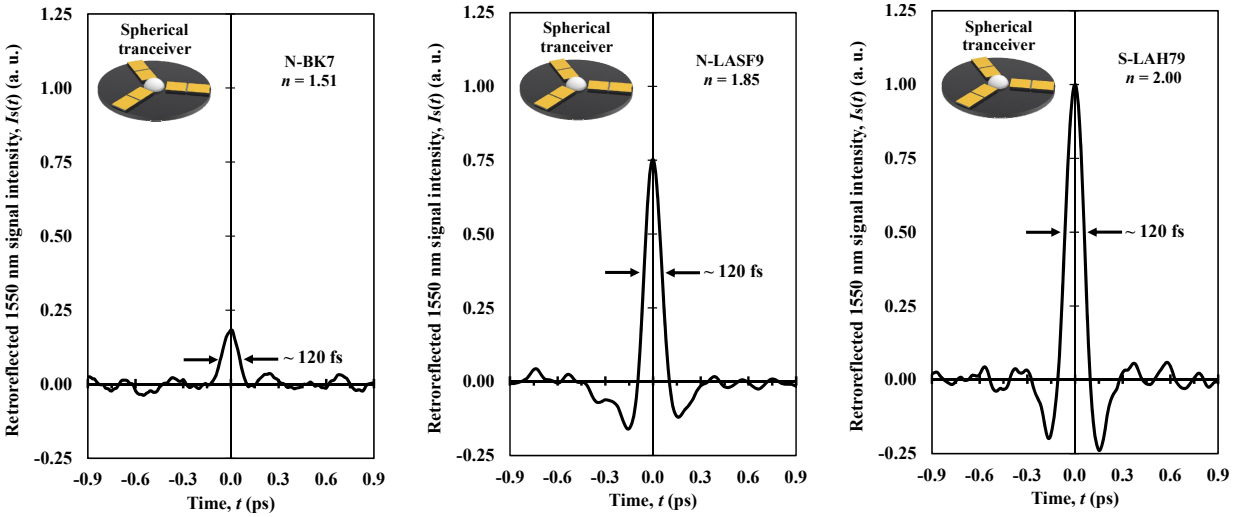

Figure 5. The retroreflected 1550 nm signal intensity, $I_s(t)$, is shown as a function of the time delay, t, for retro-modulation with (a) N-BK7 (n = 1.51), (b) N-LASF9 (n = 1.85), and (c) S-LAH79 (n = 2.00) spherical transceivers. All signal intensities are normalized with respect to the signal intensity of the S-LAH79 (n = 2.00) spherical transceiver.

Further retro-modulation studies for three spherical transceivers are carried out by varying the intensity of the local 780 nm control beam from 0.52 GW/cm^2 to 2.1 GW/cm^2. The observed retroreflected 1550 nm signal power, ΔP_s, is shown in Fig. 6, as a function of the intensity of the local 780 nm control beam for N-BK7 (n = 1.51), N-LASF9 (n = 1.85), and S-LAH79 (n = 2.00) spherical transceivers. The retroreflected 1550 nm signal powers show a linear trend, and the slope of each linear trend is used to extract nonlinear coefficients, n_2, for each glass material. For the N-BK7 (n = 1.51) spherical transceiver, the retroreflected 1550 nm signal power can only be reliably measured at the highest intensity, 2.1 GW/cm^2 of the local 780 nm control beam, and with the linear approximation, the nonlinear coefficient, n_2, is estimated to be $(3 \pm 1) \times 10^{-16}$ cm^2/W, which is on the same order as the calculated value of 3.2×10^{-16} cm^2/W from the BGO model[20]. It is also in a rough agreement with a prior experimental result[29] of 3.5×10^{-16} cm^2/W. For the N-LASF9 (n = 1.85) spherical transceiver, the retroreflected 1550 nm signal power can be reliably measured with the local 780 nm control beam intensity from 0.52 GW/cm^2 to 2.1 GW/cm^2, and the nonlinear coefficient, n_2, is estimated to be $(1.3 \pm 0.1) \times 10^{-15}$ cm^2/W. This value is on the same order as the calculated value of 1.7×10^{-15} cm^2/W from the BGO model[20] and in

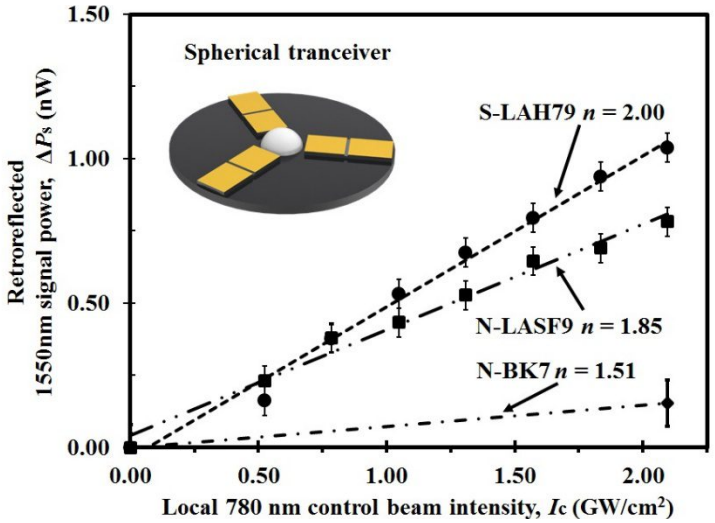

Figure 6. Retroreflected 1550 nm signal power, ΔP_s(nW), is shown as a function of the local 780 nm control beam intensity, I_c (GW/cm^2), with solid circles, squares, and diamonds for N-BK7 (n = 1.51), N-LASF9 (n = 1.85), and S-LAH79 (n = 2.00) spherical transceivers, respectively.

a rough agreement with a prior experimental result[17] of 9.6 × 10^{-16} cm^2/W. For the S-LAH79 (n = 2.00) spherical transceiver, the retroreflected 1550 nm signal power can be reliably measured with the local 780 nm control beam intensity from 0.52 GW/cm^2 to 2.1 GW/cm^2, and the nonlinear coefficient, n_2, is estimated to be (1.8 ± 0.1) × 10^{-15} cm^2/W. This value is on the same order as the calculated value of 2.8 × 10^{-15} cm^2/W from the BGO model[20]. To our knowledge, the value is unreported in the literature. Overall, the S-LAH79 (n = 2.00) spherical transceiver is best suited for OWC passive uplinks, as it enables broad angular retroreflection and high-speed all-optical modulation.

5. CONCLUSION

In this work, a transceiver was introduced for bi-directional OWC systems. The transceiver had radial PC switches for high-speed signal detection and a spherical retro-modulator for broad angular retroreflection and high-speed all-optical modulation. Theoretical models and experimental testing were used to characterize spherical transceivers comprised of glasses having differing refraction and nonlinearity. It was found that a spherical transceiver comprised of S-LAH79 yields the desired broad angular retroreflection (over a solid angle of 2π steradians) and ultrafast modulation (over a duration of 120 fs). Such spherical transceivers can enable all-optical operation in future bi-directional OWC systems.

ACKNOWLEDGEMENTS

This work is supported by the Natural Sciences and Engineering Research Council of Canada (NSERC).

REFERENCES

[1] Oh, C. W., Tangdiongga, E., and Koonen, A. M. J., "Steerable pencil beams for multi-Gbps indoor optical wireless communication," Opt. Lett. 39, 5427-5430 (2014).

[2] Wang, K., Nirmalathas, A., Lim, C., and Skafidas, E., "Ultra-broadband indoor optical wireless communication system with multimode fiber," Opt. Lett. 37, 1514-1516 (2012).

[3] Daukantas, P., "Optical wireless communications: The new hot spots," Opt. Photon. News 25, 34-41 (2014).

[4] Jin, X., and Holzman, J. F., "Multitone photoconductive sensors for free-space optics," IEEE Photon. J. 2, 659-669 (2010).

[5] Elgala, H., Mesleh, R., and Haas, H., "Indoor optical wireless communication: Potential and state-of-the-art," IEEE Commun. Mag. 49, 56-62 (2011).

[6] Minh, H. L., O'Brien, D., Faulkner, G., Zeng, L., Lee, K., Jung, D., and Oh, Y., "High-speed visible light communications using multiple-resonant equalization," IEEE Photon. Technol. Lett. 20, 1243-1245 (2008).

[7] Brandl, P., Weiss, A., and Zimmermann, H., "Automated alignment system for optical wireless communication systems using image recognition," Opt. Lett. 39, 4045-4048 (2014).

[8] Rabinovich, W. S., Mahon, R., Goetz, P. G., Waluschka, E., Katzer, D. S., Binari, S. C., and Gilbreath, G. C., "A cat's eye multiple quantum-well modulating retro-reflector," IEEE Photon. Technol. Lett. 15, 461-463 (2003).

[9] Rabinovich, W. S., Mahon, R., Burris, H. R., Gilbreath, G. C., Goetz, P. G., Moore, C. I., Stell, M. F., Vilcheck, M. J., Witkowsky, J. L., Swingen, L., Suite, M. R., Oh, E., and Koplow, J., "Free-space optical communications link at 1550 nm using multiple-quantum-well modulating retroreflectors in a marine environment," Opt. Eng. 44, 056001 (2005).

[10] Collier, C. M., Jin, X., Holzman, J. F., and Cheng, J., "Omni-directional characteristics of composite retroreflectors," J. Opt. A.: Pure Appl. Opt. 11, 085404 (2009).

[11] Rabinovich, W. S., "Modulating retro-reflection links for high bandwidth free-space lasercomm," presented at the Office of Naval Research, Arlington, USA, 8 April, (2009).

[12] Jin, X., Barg, J. E., and Holzman, J. F., "Retro-detective control structures for free-space optical communication links," Opt. Express 17, 23867-23872 (2009).

[13] Nilson, R. B., and Lu, X. J., "Optimum design of spherical retroreflectors with refractive indices close to 2.0," Trans. Inst. Meas. Control 18, 212-215 (1996).

[14] Oakley, J. P., "Whole-angle spherical retroreflector using concentric layers of homogeneous optical media," Appl. Opt. 46, 1026-1031 (2007).

[15] Zhou, L., Kahn, J. M., and Pister, K. S. J., "Corner-cube retroreflectors based on structure-assisted assembly for free-space optical communication," J. Microelectromech. Syst. 12, 233-242 (2003).

[16] O'Brien, D. C., Yuan, W. W., Liu, J. J., Faulkner, G. E., Elston, S. J., Collins, S., and Parry-Jones, L. A., "Optical wireless communications for micro-machines," Proc. SPIE 6304, 6304A (2006).

[17] Aber, J. E., Newstein, M. C., and Garetz, B. A., "Femtosecond optical kerr effect measurements in silicate glasses," J. Opt. Soc. Am. B. 17, 120-127 (2000).

[18] Born, B., Krupa, J. D. A., Geoffroy-Gagnon, S., and Holzman, J. F., "Integration of photonic nanojets and semiconductor nanoparticles for enhanced all-optical switching," Nature Commun. 6, 8097 (2015).

[19] Jin, X., Collier, C. M., Garbowski, J. J. A., Born, B., and Holzman, J. F., "Ultrafast transient responses of optical wireless communication detectors," Appl. Opt. 52, 5042-5049 (2013).

[20] Boling, N. L., Glass, A. J., and Owyoung, A., "Empirical relationships for predicting nonlinear refractive index changes in optical solids," IEEE J. Quantum Electron. QE-14, 601-608 (1978).

[21] Wang Y., and Chi, N., "Indoor gigabit 2×2 imaging multiple-input-multiple-output visible light communication," Chinese Opt. Lett. 12, 100603 (2014).

[22] Saleh, B. E. A., and Teich, M. C., [Fundamentals of Photonics], Wiley-Interscience, Chicester, (2007).

[23] Schott, [Optical Glass Data Sheets], Schott Optical Glass, Inc., 15 (2001).

[24] Schott, [Optical Glass Data Sheets], Schott Optical Glass, Inc., 75 (2001).

[25] Ohara, [Optical Glass Catalog], Ohara Corp., 6 (2007).

[26] Bernacki, B. E., Anheier, N. C., Krishnaswami, K., Cannon, B. D., and Binkley, K. B., "Design and fabrication of efficient miniature retroreflectors for the mid- and long-wave infrared," Proc. SPIE 6940, 69400X (2008).

[27] Lecler, S., Takakura, Y., and Meyrueis, P., "Properties of a three-dimensional photonic jet," Opt. Lett. 30, 2641–2643 (2005).

[28] Bergen, M. H., Nichols, J., Collier, C. M., Jin, X., Raja, B., Roberts, D. J., Ruchhoeft, P., Willson, R. C., and Holzman, J. F., "A retroreflective imaging system for optical labelling and detection of microorganisms," Appl. Opt. 53, 3647-3655 (2014).

[29] Chen, Y.-H., Varma, S., Alexeev, I., and Milchberg, H. M., "Measurement of transient nonlinear refractive index in gases using xenon supercontinuum single-shot spectral interferometry," Opt. Express 15, 7458-7467 (2007).